

Vorasidenib (AG-881): A First-in-Class, Brain-Penetrant Dual Inhibitor of Mutant IDH1 and 2 for Treatment of Glioma

Zenon Konteatis,[†] Erin Artin,^{†,‡} Brandon Nicolay,[†] Kimberly Straley,^{†,§} Anil K. Padyana,[†] Lei Jin,[†] Yue Chen,[†] Rohini Narayaraswamy,[†] Shuilong Tong,^{||} Feng Wang,[▲] Ding Zhou,^{□,≡} Dawei Cui,^{□,◇} Zhenwei Cai,[□] Zhiyong Luo,[∞] Cheng Fang,[∞] Huachun Tang,[∞] Xiaobing Lv,^{∞,#} Raj Nagaraja,[†] Hua Yang,[†] Shin-San M. Su,^{†,∇} Zhihua Sui,[†] Lenny Dang,^{†,⊕} Katharine Yen,^{†,≪} Janeta Popovici-Muller,^{†,∇} Paolo Codega,^{+,⊥} Carl Campos,⁺ Ingo K. Mellinghoff,⁺ and Scott A. Biller^{*,†}

[†]Agios Pharmaceuticals, Inc., Cambridge, Massachusetts 02139, United States

^{||}Viva Biotech, Shanghai 201203, China

[▲]Wuxi Biortus Biosciences Co. Ltd, Jiangyin 214437, China

[□]PharmaResources, Shanghai 201201, China

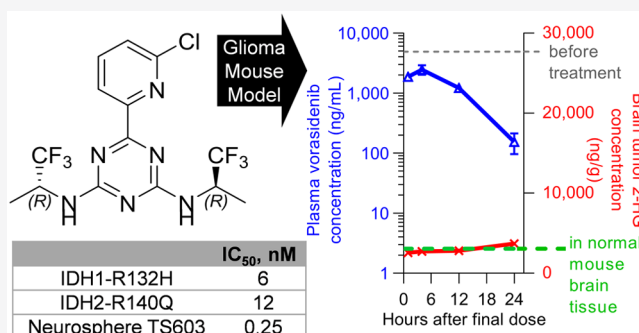
[∞]ChemPartner, Shanghai 201203, China

⁺Memorial Sloan Kettering Cancer Center, New York, New York 10065, United States

Supporting Information

ABSTRACT: Inhibitors of mutant isocitrate dehydrogenase (mIDH) 1 and 2 cancer-associated enzymes prevent the accumulation of the oncometabolite D-2-hydroxyglutarate (2-HG) and are under clinical investigation for the treatment of several cancers harboring an IDH mutation. Herein, we describe the discovery of vorasidenib (AG-881), a potent, oral, brain-penetrant dual inhibitor of both mIDH1 and mIDH2. X-ray cocrystal structures allowed us to characterize the compound binding site, leading to an understanding of the dual mutant inhibition. Furthermore, vorasidenib penetrates the brain of several preclinical species and inhibits 2-HG production in glioma tissue by >97% in an orthotopic glioma mouse model. Vorasidenib represents a novel dual mIDH1/2 inhibitor and is currently in clinical development for the treatment of low-grade mIDH glioma.

KEYWORDS: Isocitrate dehydrogenase, mutant IDH1/mIDH2, AG-881, vorasidenib, 2-hydroxyglutarate



Heterozygous mutations in cytosolic or mitochondrial isoforms of isocitrate dehydrogenase (IDH) 1 or 2, respectively, contribute to oncogenesis through the production of the oncometabolite D-2-hydroxyglutarate (2-HG).¹ Although mutant IDH (mIDH) cancers can harbor mutations in either IDH1 or IDH2, the major mIDH cancer types including acute myeloid leukemia (AML) and glioma have both mIDH1- and mIDH2-driven population subsets.^{2–4} mIDH1 and mIDH2 have also been reported in cholangiocarcinoma^{5,6} and chondrosarcoma.⁷ Two isoform-selective mIDH inhibitors that suppress 2-HG production and induce clinical responses in patients with mIDH cancers have been approved by the US Food and Drug Administration. Ivosidenib (TIBSOVO, AG-120)⁸ and enasidenib (IDHIFA, AG-221)⁹ are first-in-class inhibitors approved for the treatment of relapsed or refractory AML with an IDH1 or IDH2 mutation, respectively; ivosidenib is also approved for mIDH1 intensive chemotherapy-ineligible newly diagnosed AML.

Although ivosidenib and enasidenib are potent mIDH1 and mIDH2 inhibitors, respectively, they both exhibit low brain drug exposure in preclinical models, which could limit their potential efficacy for the treatment of mIDH glioma. Thus, we aimed to develop a mIDH1 inhibitor with good brain penetration for the treatment of glioma in which IDH1 mutations are prevalent. A recent study revealed that isoform switching from mIDH1 to mIDH2 or vice versa may represent a mechanism of acquired resistance.¹⁰ This observation provides further clinical proof that IDH is an oncogene and also suggests that the cooccurrence of mIDH1 and mIDH2 within the same tumor presents a potential therapeutic use for dual mIDH1/2 inhibitors, especially for long-term treatment such as is required for low-grade glioma. Herein, we describe

Received: November 5, 2019

Accepted: January 22, 2020

Published: January 22, 2020

the lead identification and optimization efforts that led to the discovery of vorasidenib (AG-881), a first-in-class dual mIDH1/2 inhibitor with increased brain penetration that is currently in clinical development for the treatment of low-grade glioma. We also report findings from preclinical studies describing the *in vitro* and *in vivo* characterization of vorasidenib.

The heterodimeric enzyme mIDH1-R132H/IDH1-wild type (WT) and the homodimeric enzyme mIDH2-R140Q were used for primary biochemical potency evaluation as previously described (Supporting Information).¹¹ Cellular potency profiling was routinely performed using the patient-derived neurosphere TS603 IDH1-R132H glioma-sphere line (Supporting Information) and the U87MG pLVX IDH2-R140Q engineered cell line.¹² Cell-based 2-HG inhibition was assessed by liquid chromatography–mass spectrometry quantification of 2-HG in media at 48 h. We speculated that analogs of our mIDH inhibitors with decreased topological polar surface area (tPSA) and fewer hydrogen-bond donors/acceptors would have improved ability to cross the blood–brain barrier. During the research that led to the discovery of the mIDH2 inhibitor enasidenib,¹² which has three hydrogen-bond donors, a related triazine compound with two hydrogen-bond donors (AGI-12026) was found to inhibit both mIDH2 and mIDH1 enzymes with good potency and importantly exhibited excellent brain penetration (Table 1). Both enasidenib and

Table 1. Characterization of Initial Triazine Compounds in the Hit Identification Campaign for Brain-Penetrant mIDH Inhibitors

Biochemical inhibition	Enasidenib	AGI-12026	AGI-15056
IDH1-WT/IDH1-R132H			
IC ₅₀ (μM)	0.677	0.020	0.006
IDH1-WT/IDH1-R132H maximal inhibition (%)	83	102	110
IDH1-R132H homodimer			
IC ₅₀ (μM)	4.95	0.078	0.048
IDH1-R132H homodimer maximal inhibition (%)	48	32	88
IDH2-R140Q homodimer			
IC ₅₀ (μM)	0.009	0.019	0.022
Mean mouse brain-to-plasma ratio (50 mg/kg oral dose) ^a	0.14	2.5	1.5

^aBrain-to-plasma ratio was calculated by time point measurements. Abbreviations: IDH, isocitrate dehydrogenase; mIDH, mutant isocitrate dehydrogenase; WT, wild type.

AGI-12026 show partial inhibition of the IDH1-R132H homodimer (Table 1) as allosteric modulators have been known to induce both full and intermediate structural changes in the active site of enzymes resulting in varying degrees of efficacy.¹³ To evaluate preliminary structure–activity–relationships (SAR), we screened all the triazine compounds in our collection to identify potential brain-penetrating small-molecule inhibitors of mIDH1 and mIDH2.

Several of the triazine compounds showed good inhibitory activity against both mIDH1-R132H and mIDH2-R140Q enzymes and substantial brain exposure relative to plasma concentration in mouse pharmacokinetic studies. One compound, AGI-15056, effectively inhibited both enzymes, with a brain-to-plasma ratio of 1.5 (Table 1). Furthermore, AGI-15056 potently inhibited the heterodimer IDH1-WT/IDH1-R132H enzyme and demonstrated excellent potency in neurosphere TS603 IDH1-R132H and U87MG IDH2-R140Q mutant cell assays (Table 3).

The chemical structure of AGI-15056 is characterized by an aryl ring system in the 6-position of the triazine along with two aliphatic amines in the 2- and 4-positions of the scaffold. Other compounds that showed dual mIDH1/2 inhibitory activity shared this overall motif, so synthetic efforts focused on this subclass. The synthetic scheme used to generate these analogs is described in Supporting Information Scheme S1. The other two isomers of AGI-15056 (*R, R*), compounds **1** (*S, R*) and **2** (*S, S*) showed slightly less potency in all biochemical and cell assays (Supporting Information Table S1). Therefore, emphasis was given to the (*R, R*) isomers in the SAR development. Periodic syntheses of all relevant isomers were conducted for key analogs (data not reported), and the trend for the (*R, R*)-isomer to have superior potency was maintained.

The cocrystal structure of AGI-15056 in complex with mIDH1-R132H (IDH1-R132H-NADPH·AGI-15056) was determined at 2.66 Å resolution to enable structure-based design (Supporting Information Table S2). AGI-15056 binds in the previously described allosteric tetrahelical center of the IDH1-R132H obligate dimer interface¹⁴ and is captured in an alternative conformation with pseudosymmetric pose, similar to the enasidenib crystal structure with IDH2-R140Q (Figure 1).¹² As with the enasidenib/IDH2-R140Q complex, the

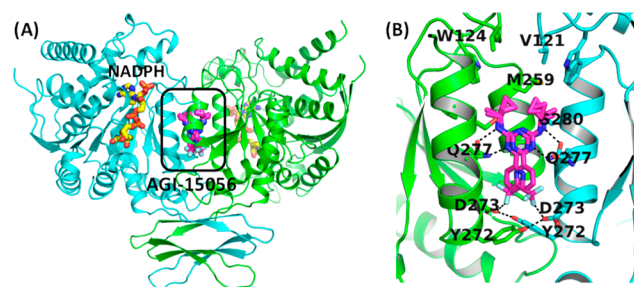


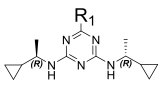
Figure 1. (A) Cocrystal structure of AGI-15056 in complex with IDH1-R132H homodimer. mIDH1 is in the inhibitory open homodimer conformation. (B) Close-up of the allosteric site; helix 9' has been removed for clarity. AGI-15056 shows two possible pseudosymmetric binding conformations. Abbreviations: IDH, isocitrate dehydrogenase; mIDH, mutant isocitrate dehydrogenase.

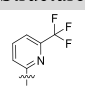
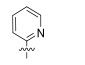
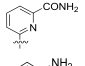
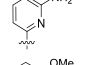
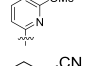
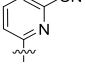
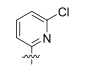
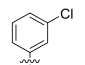
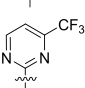
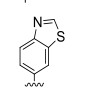
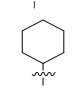
mIDH1 protein here is in the open inactive state. The triazine inhibitor binding pocket is surrounded by four helices ($\alpha 9$, $\alpha 10$, $\alpha 9'$, $\alpha 10'$) along the sides and by two loops (L1, L1'), with the Y272–D273 interaction pairs capping the ends. The aminotriazine core interacts via hydrogen bonds with the side chains of the two Q277 residues, which point into the interior of the pocket, whereas the majority of the inhibitor is surrounded by hydrophobic residues (V121, W124, I251, V255, M259, and W267) and interacts via van der Waals contacts. The other hydrophilic residue in the binding site (S280) does not interact with the inhibitor. The trifluoromethyl group of AGI-15056 interacts with the D273 oxygen

via a carbon–fluoride–oxygen bond (tetrel σ bond),¹⁵ and the alternate poses showcase this interaction on both sides of the symmetric pocket. The similar binding pocket arrangement exhibited by this inhibitor and enasidenib/IDH2-R140Q, and the specific interactions common to both systems, explain the observed affinity of AGI-15056 to both mIDH1 and mIDH2 enzymes. The majority of residues in the binding site are conserved between mIDH1 and mIDH2. Structural comparison suggests that enasidenib interacts with mIDH2-specific hydrophobic residue pairs V297, L298, I319, and L320 (compared with A258, M259, S280, and V281 for mIDH1), which likely explains its selectivity. The symmetry of inhibitor binding, the mostly hydrophobic pocket environment, and the similarities and differences observed in the specific interactions were major insights that became the central theme in our SAR exploration.

Using these insights into the inhibitor–protein interactions and the binding site characteristics, several compounds were synthesized to examine the SAR of the triazine series. First, the R₁ substitution at the C-6 position was examined for optimal binding (Table 2). Removing the CF₃ substituent led to a great loss in potency (3), as did substitutions of the CF₃ group by

Table 2. Biochemical Activity of R₁ Modifications of AGI-15056^a



Compound	Structure	IDH1-WT/IDH1-R132H IC ₅₀ (μM)
AGI-15056		0.006
3		1.566
4		1.749
5		0.394
6		0.677
7		0.201
8		0.032
9		0.14
10		0.185
11		No fit
12		No fit

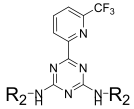
^aNo fit = no measurable inhibition for proper curve-fitting. Abbreviations: IDH, isocitrate dehydrogenase; WT, wild type.

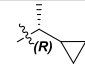
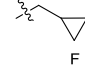

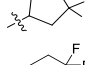
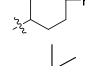
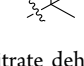
various polar substituents (4, 5, 6, and 7). Only replacement of this group by a chlorine (8) maintained potency within 5-fold levels. Removing the nitrogen from the chloropyridine led to further potency loss (9). Adding a second nitrogen in the R₁ ring in the 5-position (10) gave a weaker IC₅₀, whereas adding a bicyclic system (11) or saturating the R₁ ring (12) completely abolished binding to mIDH1.

Second, the R₂, R₂' symmetrical substitution was studied, keeping the CF₃-pyridine in R₁ (Table 3). Removing the methyl group from the AGI-15056 analog (13) resulted in a loss of enzymatic potency but not cellular potency. Difluorocyclobutyl (14) and difluorocyclopentyl (15) analogs had nanomolar potency against both mIDH1 and mIDH2 and maintained good potency in both cell assays. The difluorocyclohexyl substitution (16) led to reduced enzymatic potency but good cellular activity. The *tert*-butyl substitution (17) led to weaker activities. These results are consistent with the insights from the cocrystal structure, suggesting that lipophilicity drives the binding site. Finally, as the only other R₁ substituent that exhibited good potency was 2-Cl-pyridine (8; Table 2), a series of analogs were synthesized with this substituent using the best R₂, R₂' from the CF₃-pyridine system (Table 4). Compound 18 showed good enzymatic potency and cellular activity, especially in the neurosphere TS603 cell assay. Compound 19, reflecting the results from the series shown in Table 3, was less potent in all assays, and compounds 20 and 21 (the ethyl analog of 20) had similar potency. The trifluoro-2-methylpropane substitution (22) showed excellent inhibition in the neurosphere TS603 cell assay, which led to the study of its stereoisomers. All three isomers (23, 24, and vorasidenib) had nanomolar potency in the heterodimer mIDH1 enzymatic assay, and vorasidenib (*R, R* isomer) had slightly better potency in the cell assays (Supporting Information Table S3), which suggests biochemical assay conditions did not fully capture residence time that translated to better cellular potency. In rat pharmacokinetic studies, vorasidenib and compound 24 showed brain-to-plasma ratios of 0.65 and 0.46, respectively. At this point vorasidenib was selected for further profiling to evaluate its potential as a clinical candidate for the treatment of glioma.

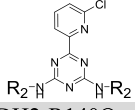
A number of key molecules in the program were tested for brain penetration in mice (Supporting Information Table S4). All compounds that showed brain-to-plasma ratios between 0.65 and 2.5 had tPSA values between 73 and 86 Å². These values fall within the traditionally accepted guidelines for brain-penetrant molecules.^{16,17} However, enasidenib, which has a low brain-to-plasma ratio of 0.14, is more polar with a tPSA of 106 Å². Enasidenib has three hydrogen-bond donors, whereas all the other molecules have two hydrogen-bond donors, indicating that up to two hydrogen-bond donors in the molecules were acceptable for brain penetration, perhaps because of the overall low tPSA and higher logarithm of partition coefficient between *n*-octanol and water (logP). All compounds tested had clogP > 3, reflecting the very hydrophobic binding site of the mIDH1 protein.

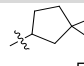
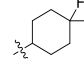

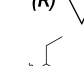
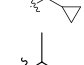
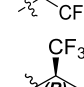
As vorasidenib and its congeners are the first dual mIDH1/2 inhibitors reported to date, we determined the cocrystal structures of vorasidenib in complex with NADPH-bound forms of IDH1-R132H and IDH2-R140Q homodimers at 2.1 and 1.99 Å resolution, respectively (Supporting Information Table S2). The two sets of crystal structures are very similar with minor differences. Vorasidenib binds both IDH1-R132H and IDH2-R140Q in the same allosteric pocket at the interface

Table 3. Biochemical and Cellular Activities of R₂ Symmetrical Analogs^a


Compound	Structure	IDH1-R132H/IDH1-WT	IDH2-R140Q	Neurosphere TS603	U87 IDH2-R140Q
		IC ₅₀ (μM)	IC ₅₀ (μM)	mIDH1-R132H IC ₅₀ (μM)	IC ₅₀ (μM)
AGI-15056		0.006	0.022	0.002	0.014
13		0.083	0.013	NT	0.022
14		0.009	0.016	0.001	0.003
15		0.006	NT	0.001	0.009
16		0.027	0.092	0.004	0.009
17		0.060	0.046	NT	NT

^aAbbreviations: IDH, isocitrate dehydrogenase; mIDH, mutant isocitrate dehydrogenase; NT, not tested; WT, wild type.

Table 4. Biochemical and Cellular Activities of R₂ Analogs with a 2-Cl-Pyridyl R₁ Substituent^a


Compound	Structure	IDH1-R132H/IDH1-WT	Neurosphere TS603	U87 IDH2-R140Q
		IC ₅₀ (μM)	IDH1-R132H IC ₅₀ (μM)	IC ₅₀ (μM)
18		0.006	0.0007	0.006
19		0.022	0.007	0.022
20		0.009	NT	0.004
21		0.006	0.004	0.014
22		0.007	0.0003	0.008
Vorasidenib (AG-881)		0.0006	0.00025	0.007

^aAbbreviations: IDH, isocitrate dehydrogenase; NT, not tested; WT, wild type.

of the two monomers formed by two helices from each monomer, in a symmetrical fashion (Figure 2 and Supporting Information Figure S1). This was previously disclosed by another report¹⁸ and also described for enasidenib,¹² as discussed earlier for AGI-15056.

The three crystal structures show that both enzymes are in the open inhibited conformational states. Both hydrophilic and hydrophobic interactions drive the affinity of vorasidenib with both mIDH1 and mIDH2 proteins. Analysis of electron density suggested one conformation for the vorasidenib molecule for each IDH1-R132H dimer, and its specific interactions include the side chains of Q277 forming hydrogen bonds with the aminotriazine core on either side (Figure 2A and Supporting Information Figure S1A). A halogen bond

exists between the chlorine atom of the chloropyridine moiety of vorasidenib and the carbonyl of D273 that is part of the capping residues. Three other fluorine–oxygen bonds exist between the aliphatic CF₃ and the carbonyl oxygen of Q277 on one side, between the backbone carbonyl of V255 and the same CF₃, and between the other CF₃ to the backbone carbonyl of V255' on the other portion of the symmetric pocket. Vorasidenib also makes multiple van der Waals contacts with the side chains of residues W124, M259, V255, V276, and W267.

In comparison, two alternative conformations of vorasidenib could be modeled in the IDH2-R140Q cocrystal structure that exhibit the same hydrogen bonding interactions between the aminotriazine core of vorasidenib and the side chains of the

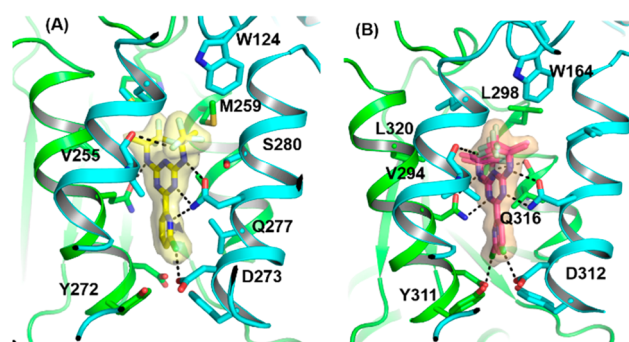


Figure 2. Cocystal structure of vorasidenib in complex with (A) IDH1-R132H with a single conformation fit and (B) IDH2-R140Q with two alternate conformation fits. The electron density around vorasidenib is contoured at 1.0σ using a $2mF_o - DF_c$ map shown as a surface envelope along with the polar interactions to the binding site residues shown as dashed lines. Abbreviation: IDH, isocitrate dehydrogenase.

two Q316 residues (Figure 2B and Supporting Information Figure S1B). The chlorine atom of the chloropyridine group of vorasidenib maintains the same halogen σ bond with the carbonyl of D312 for each copy of the inhibitor. Two weaker bonds are also formed between the aliphatic CF_3 group and the backbone carbonyls of V294 and V294'. van der Waals interactions complete the hydrophobic binding between vorasidenib and residues W164, V294, V297, L298, V315, I319, and L320, similar to those reported for enasidenib.¹²

Consistent with X-ray crystallographic results showing optimized interactions of the inhibitor within the enzyme allosteric binding pockets of mIDH1 and mIDH2, vorasidenib possesses good biochemical potency against both mIDH1 and mIDH2 isoforms (Supporting Information Tables S5 and S6). Interestingly, inhibition against mIDH1 showed rapid-equilibrium characteristics, whereas inhibition against IDH1-WT or mIDH2 isoforms showed time-dependent characteristics, likely reflecting differences between mIDH1, IDH1-WT, and mIDH2 protein dynamics. Vorasidenib also demonstrated excellent *in vivo* suppression of 2-HG production in cultured neurospheres harboring IDH1-R132H (Supporting Information Table S7). Importantly, vorasidenib also exhibited sustained exposure and high brain-to-plasma ratios across a range of preclinical species (Figure 3 and Supporting Information Table S8).

To evaluate the activity of vorasidenib in a patient-derived xenograft model in mouse brain, mice were inoculated

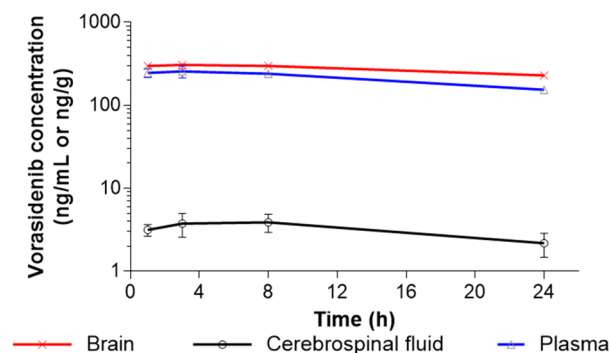


Figure 3. Vorasidenib concentrations in plasma, brain, and cerebrospinal fluid (3 mg/kg single oral dose in rats; $n = 3$).

orthotopically with TS603 IDH1-R132H grade III glioma cells and monitored until tumor volumes were estimated to be $\sim 40 \text{ mm}^3$ by magnetic resonance imaging measurement. Mice were then randomly assigned and dosed every 12 h for 4 days with either vehicle alone or vorasidenib at 50 mg/kg. After eight repeat doses, animals were sacrificed at the indicated time points after the last dose, and the relationship between vorasidenib exposure in the brain and plasma and inhibition of 2-HG production was determined (Figure 4). Vorasidenib treatment led to a $>97\%$ inhibition of 2-HG production in the mIDH1 glioma tissue. The brain-to-plasma area under the curve ratio (calculated using total concentration of tumor plus brain tissue) was 1.33 and the brain tumor-to-plasma area under the curve ratio was 1.25.

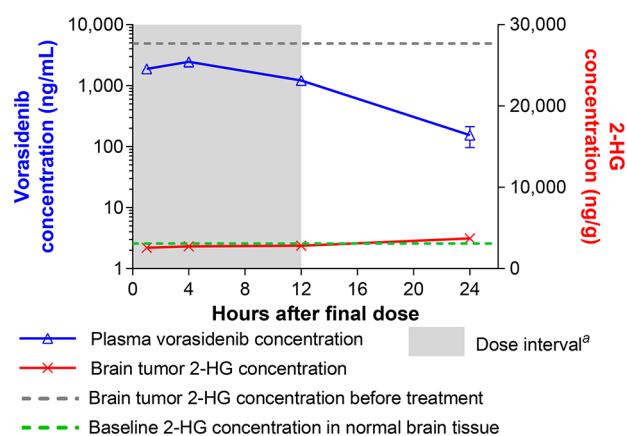


Figure 4. Vorasidenib (AG-881) inhibited 2-HG levels in an orthotopic grade III mIDH1 glioma model derived from the TS603 neurosphere. Dose: 50 mg/kg by mouth twice daily for 4 days. "Grayed area represents the dose interval; the 24-h time point was included to assess how long 2-HG inhibition was sustained in the brain tumor after the last dose. %2-HG inhibition was established after subtracting 2-HG AUC_{0-12h} of "normal" brain (observed in left hemisphere of brains in all animals), from brain tumor AUC_{0-12h} . Gray dashed line represents the 2-HG concentrations in the brain tumors of untreated animals. Abbreviations: 2-HG, D-2-hydroxyglutarate; AUC_{0-12h} , area under the curve from 0 to 12 h; mIDH, mutant isocitrate dehydrogenase.

The triazine enasidenib and closely related analogs are selective for mIDH2 over mIDH1, and they generally showed poor brain-to-plasma ratios. However, on broader evaluation of the triazine analogs, we found that potent inhibitors with two hydrogen bond donors can be designed to possess properties for effective brain penetration. We also observed that certain symmetrical N,N' -dialkyl analogs showed equipotent inhibitory activity against mIDH1 and mIDH2. Cocomplex structures of these compounds with mIDH1 revealed a similar binding mode in the same allosteric pocket analogous to mIDH2, both of which are highly symmetrical and characterized by four α -helices and two small loops to cap the pocket boundary. These key observations guided our rational design of triazines for dual-inhibitory properties. Indeed, optimization of small symmetrical N,N' -dialkyl triazines achieved both high brain-to-plasma ratios and comparable mIDH1/2 isoform inhibition, ultimately leading to the discovery of vorasidenib. Vorasidenib demonstrated excellent biochemical inhibition against mIDH1 and mIDH2 and inhibited 2-HG production in cultured TS603 neuro-

spheres derived from a patient with grade III glioma harboring an IDH1-R132H mutation. Following oral dosing, vorasidenib also led to complete suppression of 2-HG levels in the orthotopic patient-derived xenograft TS603 glioma model in mice brains.

Vorasidenib is a promising brain-penetrant dual mIDH1/2 inhibitor under late-stage development for the treatment of low-grade mIDH glioma, and it has shown promising clinical activity in early clinical trials ([ClinicalTrials.gov](https://clinicaltrials.gov/ct2/show/study/NCT02481154) NCT02481154¹⁹ and [ClinicalTrials.gov](https://clinicaltrials.gov/ct2/show/study/NCT03343197) NCT03343197).²⁰ Vorasidenib was recently reported to reduce 2-HG levels by >90% in mIDH gliomas in humans, as demonstrated by analysis of postdrug treatment tumor samples obtained by resection in a perioperative study ([ClinicalTrials.gov](https://clinicaltrials.gov/ct2/show/study/NCT03343197) NCT03343197).²⁰ These clinical results validate the preclinical characterization reported herein.

■ ASSOCIATED CONTENT

Supporting Information

The Supporting Information is available free of charge at <https://pubs.acs.org/doi/10.1021/acsmchemlett.9b00509>.

Supplementary figures, tables, experimental details, and abbreviations (PDF)

Accession Codes

The coordinates of the crystal structures have been deposited to the RCSB Protein Data Bank under the following accession codes: 6VEI (IDH1-R132H-NADPH-AG-881), 6VFZ (IDH2-R140Q-NADPH-AG-881), and 6VG0 (IDH1-R132H-NADPH-AGI-15056).

■ AUTHOR INFORMATION

Corresponding Author

*Email: scott.biller@agios.com.

ORCID

Lenny Dang: 0000-0002-2073-6109

Present Addresses

[‡]KSQ Therapeutics, Cambridge, MA 02139, USA.

[§]Vertex Pharmaceuticals, Boston, MA 02210, USA.

[≡]Zion Pharma, Shanghai 200000, China.

[◇]Suzhou Zelgen Biopharmaceuticals, Kunshan 215300, China

[⊥]Sundia, Shanghai 201203, China.

[∩]Decibel Therapeutics, Cambridge, MA 02215, USA.

[≪]Auron Therapeutics, Wellesley, MA 02481, USA.

[#]Italfarmaco SpA, Cinisello Balsamo 20092, Italy.

Author Contributions

The manuscript was written through contributions of all authors. All authors approved the final version of the manuscript.

Funding

These studies were funded by Agios Pharmaceuticals, Inc.

Notes

The authors declare the following competing financial interest(s): All Agios authors were employees and stockholders at the time of the study.

■ ACKNOWLEDGMENTS

Editorial assistance was provided by Christine Ingleby, PhD, CMPP, of Excel Medical Affairs, Horsham, UK, and supported by Agios Pharmaceuticals, Inc.

■ ABBREVIATIONS

2-HG, D-2-hydroxyglutarate; AML, acute myeloid leukemia; AUC_{0–12h}, area under the curve from 0 to 12 h; CSF, cerebrospinal fluid; IDH, isocitrate dehydrogenase; mIDH, mutant isocitrate dehydrogenase; SAR, structure–activity–relationships; tPSA, topological polar surface area; WT, wild type.

■ REFERENCES

- (1) Dang, L.; Yen, K.; Attar, E. C. IDH mutations in cancer and progress toward development of targeted therapeutics. *Ann. Oncol.* **2016**, *27* (4), 599–608.
- (2) Yan, H.; Parsons, D. W.; Jin, G.; McLendon, R.; Rasheed, B. A.; Yuan, W.; Kos, I.; Batinic-Haberle, I.; Jones, S.; Riggins, G. J.; Friedman, H.; Friedman, A.; Reardon, D.; Herndon, J.; Kinzler, K. W.; Velculescu, V. E.; Vogelstein, B.; Bigner, D. D. IDH1 and IDH2 mutations in gliomas. *N. Engl. J. Med.* **2009**, *360* (8), 765–773.
- (3) Ward, P. S.; Patel, J.; Wise, D. R.; Abdel-Wahab, O.; Bennett, B. D.; Collier, H. A.; Cross, J. R.; Fantin, V. R.; Hedvat, C. V.; Perl, A. E.; Rabinowitz, J. D.; Carroll, M.; Su, S. M.; Sharp, K. A.; Levine, R. L.; Thompson, C. B. The common feature of leukemia-associated IDH1 and IDH2 mutations is a neomorphic enzyme activity converting alpha-ketoglutarate to 2-hydroxyglutarate. *Cancer Cell* **2010**, *17* (3), 225–234.
- (4) Parsons, D. W.; Jones, S.; Zhang, X.; Lin, J. C.; Leary, R. J.; Angenendt, P.; Mankoo, P.; Carter, H.; Siu, I. M.; Gallia, G. L.; Olivari, A.; McLendon, R.; Rasheed, B. A.; Keir, S.; Nikolskaya, T.; Nikolsky, Y.; Busam, D. A.; Tekleab, H.; Diaz, L. A., Jr.; Hartigan, J.; Smith, D. R.; Strausberg, R. L.; Marie, S. K.; Shinjo, S. M.; Yan, H.; Riggins, G. J.; Bigner, D. D.; Karchin, R.; Papadopoulos, N.; Parmigiani, G.; Vogelstein, B.; Velculescu, V. E.; Kinzler, K. W. An integrated genomic analysis of human glioblastoma multiforme. *Science* **2008**, *321* (5897), 1807–1812.
- (5) Borger, D. R.; Tanabe, K. K.; Fan, K. C.; Lopez, H. U.; Fantin, V. R.; Straley, K. S.; Schenkein, D. P.; Hezel, A. F.; Ancukiewicz, M.; Liebman, H. M.; Kwak, E. L.; Clark, J. W.; Ryan, D. P.; Deshpande, V.; Dias-Santagata, D.; Ellisen, L. W.; Zhu, A. X.; Iafate, A. J. Frequent mutation of isocitrate dehydrogenase (IDH)1 and IDH2 in cholangiocarcinoma identified through broad-based tumor genotyping. *Oncologist* **2012**, *17* (1), 72–79.
- (6) Farshidfar, F.; Zheng, S.; Gingras, M. C.; Newton, Y.; Shih, J.; Robertson, A. G.; Hinoue, T.; Hoadley, K. A.; Gibb, E. A.; Roszik, J.; Covington, K. R.; Wu, C. C.; Shinbrot, E.; Stransky, N.; Hegde, A.; Yang, J. D.; Reznik, E.; Sadeghi, S.; Pedomallu, C. S.; Ojesina, A. I.; Hess, J. M.; Auman, J. T.; Rhie, S. K.; Bowlby, R.; Borad, M. J.; Zhu, A. X.; Stuart, J. M.; Sander, C.; Akbani, R.; Cherniack, A. D.; Deshpande, V.; Mounajjed, T.; Foo, W. C.; Torbenson, M. S.; Kleiner, D. E.; Laird, P. W.; Wheeler, D. A.; McRee, A. J.; Bathe, O. F.; Andersen, J. B.; Bardeesy, N.; Roberts, L. R.; Kwong, L. N. Cancer Genome Atlas Network, Integrative genomic analysis of cholangiocarcinoma identifies distinct IDH-mutant molecular profiles. *Cell Rep* **2017**, *18* (11), 2780–2794.
- (7) Amary, M. F.; Bacsí, K.; Maggiani, F.; Damato, S.; Halai, D.; Berisha, F.; Pollock, R.; O'Donnell, P.; Grigoriadis, A.; Diss, T.; Eskandarpour, M.; Presneau, N.; Hogendoorn, P. C.; Futreal, A.; Tirabosco, R.; Flanagan, A. M. IDH1 and IDH2 mutations are frequent events in central chondrosarcoma and central and periosteal chondromas but not in other mesenchymal tumours. *J. Pathol.* **2011**, *224* (3), 334–343.
- (8) Agios Pharmaceuticals Inc. TIBSOVO [prescribing information]. <http://www.tibsovopro.com/pdf/prescribinginformation.pdf> (accessed January 30, 2020).
- (9) Celgene. IDHIFA [prescribing information]. <https://media.celgene.com/content/uploads/idhifa-pi.pdf> (accessed 20 March 2019).
- (10) Harding, J. J.; Lowery, M. A.; Shih, A. H.; Schwartzman, J. M.; Hou, S.; Famulare, C.; Patel, M.; Roshal, M.; Do, R. K.; Zehir, A.; You, D.; Selcuklu, S. D.; Viale, A.; Tallman, M. S.; Hyman, D. M.;

Reznik, E.; Finley, L. W. S.; Papaemmanuil, E.; Tosolini, A.; Frattini, M. G.; MacBeth, K. J.; Liu, G.; Fan, B.; Choe, S.; Wu, B.; Janjigian, Y. Y.; Mellinghoff, I. K.; Diaz, L. A.; Levine, R. L.; Abou-Alfa, G. K.; Stein, E. M.; Intlekofer, A. M. Isoform switching as a mechanism of acquired resistance to mutant isocitrate dehydrogenase inhibition. *Cancer Discovery* **2018**, *8* (12), 1540–1547.

(11) Popovici-Muller, J.; Lemieux, R. M.; Artin, E.; Saunders, J. O.; Salituro, F. G.; Travins, J.; Cianchetta, G.; Cai, Z.; Zhou, D.; Cui, D.; Chen, P.; Straley, K.; Tobin, E.; Wang, F.; David, M. D.; Penard-Lacronique, V.; Quivoron, C.; Saada, V.; de Botton, S.; Gross, S.; Dang, L.; Yang, H.; Utley, L.; Chen, Y.; Kim, H.; Jin, S.; Gu, Z.; Yao, G.; Luo, Z.; Lv, X.; Fang, C.; Yan, L.; Olaharski, A.; Silverman, L.; Biller, S.; Su, S. M.; Yen, K. Discovery of AG-120 (ivosidenib): a first-in-class mutant IDH1 inhibitor for the treatment of IDH1 mutant cancers. *ACS Med. Chem. Lett.* **2018**, *9* (4), 300–305.

(12) Yen, K.; Travins, J.; Wang, F.; David, M. D.; Artin, E.; Straley, K.; Padyana, A.; Gross, S.; DeLaBarre, B.; Tobin, E.; Chen, Y.; Nagaraja, R.; Choe, S.; Jin, L.; Konteatis, Z.; Cianchetta, G.; Saunders, J. O.; Salituro, F. G.; Quivoron, C.; Opolon, P.; Bawa, O.; Saada, V.; Paci, A.; Broutin, S.; Bernard, O. A.; de Botton, S.; Marteyn, B. S.; Pilichowska, M.; Xu, Y.; Fang, C.; Jiang, F.; Wei, W.; Jin, S.; Silverman, L.; Liu, W.; Yang, H.; Dang, L.; Dorsch, M.; Penard-Lacronique, V.; Biller, S. A.; Su, S. M. AG-221, a first-in-class therapy targeting acute myeloid leukemia harboring oncogenic IDH2 mutations. *Cancer Discovery* **2017**, *7* (5), 478–493.

(13) Verespy, S., 3rd; Mehta, A. Y.; Afosah, D.; Al-Horani, R. A.; Desai, U. R. Allosteric partial inhibition of monomeric proteases. Sulfated coumarins induce regulation, not just inhibition, of thrombin. *Sci. Rep.* **2016**, *6*, 24043.

(14) Deng, G.; Shen, J.; Yin, M.; McManus, J.; Mathieu, M.; Gee, P.; He, T.; Shi, C.; Bedel, O.; McLean, L. R.; Le-Strat, F.; Zhang, Y.; Marquette, J. P.; Gao, Q.; Zhang, B.; Rak, A.; Hoffmann, D.; Rooney, E.; Vassort, A.; Englaro, W.; Li, Y.; Patel, V.; Adrian, F.; Gross, S.; Wiederschain, D.; Cheng, H.; Licht, S. Selective inhibition of mutant isocitrate dehydrogenase 1 (IDH1) via disruption of a metal binding network by an allosteric small molecule. *J. Biol. Chem.* **2015**, *290* (2), 762–774.

(15) García-LLinás, X.; Bauzá, A.; Seth, S. K.; Frontera, A. Importance of R–CF₃...O tetrel bonding interactions in biological systems. *J. Phys. Chem. A* **2017**, *121* (28), 5371–5376.

(16) Mikitsh, J. L.; Chacko, A. M. Pathways for small molecule delivery to the central nervous system across the blood-brain barrier. *Perspect. Med. Chem.* **2014**, *6*, 11–24.

(17) Hitchcock, S. A.; Pennington, L. D. Structure-brain exposure relationships. *J. Med. Chem.* **2006**, *49* (26), 7559–7583.

(18) Ma, R.; Yun, C. H. Crystal structures of pan-IDH inhibitor AG-881 in complex with mutant human IDH1 and IDH2. *Biochem. Biophys. Res. Commun.* **2018**, *503* (4), 2912–2917.

(19) Mellinghoff, I. K.; Penas-Prado, M.; Peters, K. B.; Cloughesy, T. F.; Burris, H. A.; Maher, E. A.; Janku, F.; Cote, G. M.; Fuente, M. I. D. L.; Clarke, J.; Steelman, L.; Le, K.; Zhang, Y.; Sonderfan, A.; Hummel, D.; Schoenfeld, S.; Yen, K.; Pandya, S. S.; Wen, P. Y. Phase 1 study of AG-881, an inhibitor of mutant IDH1/IDH2, in patients with advanced IDH-mutant solid tumors, including glioma. *J. Clin. Oncol.* **2018**, *36* (15) (suppl), 2002.

(20) Mellinghoff, I. K.; Cloughesy, T. F.; Wen, P. Y.; Taylor, J. W.; Maher, E. A.; Arrillaga-Romany, I.; Peters, K. B.; Choi, C.; Ellingson, B. M.; Lin, A. P.; Thakur, S. B.; Nicolay, B.; Lu, M.; Le, K.; Yin, F.; Tai, F.; Schoenfeld, S.; Steelman, L.; Pandya, S. S.; Clarke, J. L. A phase 1, open-label, perioperative study of ivosidenib (AG-120) and vorasidenib (AG-881) in recurrent IDH1 mutant, low-grade glioma: Updated results. *Neuro-Oncol.* **2019**, *21* (Suppl_6), vi28–29, ACTR-66.